USERS MANUAL

NOAA/NESDIS Multiplatform Tropical Cyclone Surface Wind Analysis

Last Updated: August 30, 2010

John A. Knaff and Mark DeMaria, NESDIS/STAR

USERS MANUAL Table of Contents

1. Overview of Users Manual

This document provides a description of the multiplatform tropical cyclone surface wind analysis (MTCSWA) product, which produces six-hourly estimates of tropical cyclone wind fields based on a variety of satellite based winds and wind proxies. The product is hosted at http://www.ssd.noaa.gov/PS/TROP/mtcswa.html. In the following sections the algorithm, products, and product verification is described.

The main MTCSWA product is the estimation of the surface wind field around active tropical cyclones. The product domain is global and the active storms are determined by areas of interest (invests) and storms that have reached an intensity which triggers warnings in that basin. This information comes from several operational tropical cyclone warning centers. For this product the Joint Typhoon Warning Center, Honolulu, HI provides locations/intensities of active systems in the Southern Hemisphere, Indian Ocean, and western North Pacific, the NCEP Central Pacific Hurricane Center, Honolulu, HI provides locations/intensities for the North Central Pacific, and the NCEP Tropical Prediction Center in Miami, Florida provides location and intensities in the Eastern North Pacific and North Atlantic Basins. An important note is that this product is generated when these tropical cyclone centers ask for model guidance, and that the numbering/naming conventions follow those of the warning center providing the information and are basin specific.

This product was created by Dr. John Knaff at the NESDIS Center for Satellite Applications and Research (STAR) Regional and Mesoscale Meteorology Branch (RAMMB) located in Fort Collins, Colorado. He can be reached at John.Knaff@noaa.gov.

1. Algorithm Description

Several satellite-based estimates of near surface winds are used to create this product. These come in two general categories and at two different atmospheric levels. The categories are 1) wind fields created for general use and 2) those specifically created for tropical cyclone problems. Winds are also available at the surface (typically 10m – marine exposure) and at low levels, typically between 925 hPa and 600 hPa, which will hereafter be referred to as "flight-level". Each of these datasets has its own characteristics and shortcomings. In this section, each of these data types and how they are combined to form a single flight-level dataset is discussed. The resulting dataset is the input for an analysis, which is also discussed in this section. Table 2.1 summarizes the datasets and real-time source used in this study that is discussed below.

Table 2.1: A list describing the input datasets used to create the MTCSWA product. Data type, sensor, data source and typical pressure levels used are provided.

Data Type	Sensor	Source	Pressure Levels
Non-linear Balance winds from the Advanced Microwave	NOAA-15,16, 18	NCEP (via ftp)	850,700 hPa

Sounding Unit (AMSU)			
Cloud Drift Winds (CDFT)	Geostationary Satellites	NESDIS (GOES –E,-W, MT-Sat NRL, Monterey (EUMETSAT, JMA)	Below 600 hPa
Water Vapor Winds (WV)	Geostationary Satellites	NESDIS (GOES –E,-W, MT-Sat NRL, Monterey (EUMETSAT, JMA)	Below 600 hPa
Infrared Flight-Level Proxy Winds (IRWD)	Geostationary Satellites	NESDIS	700, 850 hPa depending on intensity
Quikscat (SCAT)[1]	Sea-Winds	NESDIS	Surface (10-m)
A-SCAT (ASCT)	MetOP 2A	NESDIS	Surface (10-m)

1.1. Satellite-based surface wind estimates

Presently this study makes use of two satellite-based surface wind sources and both are active radar instruments or scatterometry. At this time, only the oceanic wind vectors (OWV) are being utilized from the SeaWinds instrument on the QuikSCAT satellite (hereinafter QuikSCAT) and the Advance Scatterometer (ASCAT; EUMETSAT, 2010) on board the METOP -2A satellite. The WINDSAT (Gaiser 2004) surface winds are not yet utilized. QuikSCAT is a k-band (13.4 GHz) radar that senses ocean roughness. The rougher the ocean surface is the greater the wind speed estimate with a maximum wind speed design limit of 30 ms^{-1}. Two beams are 6 degrees apart that allow for the determination of wind directions (Graf et al 1998). The k-band frequency of QuikSCAT also has difficulties determining wind direction in heavy precipitation and high wind speed regimes like the tropical cyclone. Hennon et al. (2006) found that OWV in the core region are less useful than those in the surroundings and that the QuikSCAT winds are very useful for the determination of 34-knot (kt; nautical miles per hour, where 1 kt=1.85 km/h) wind radii. The ASCAT on the other hand is a c-band (5.225GHz) that senses ocean roughness. The c-band is less sensitive to precipitation than the k-band, but has lower resolution (~25 km) (Gelsthorpe et al. 2000). The larger footprints of ASCAT have resulted in a low wind bias for high winds (Bentamy et al. 2008; Cobb et al. 2008), which will be discussed in the following sections. For this product ASCT surface winds are increased uniformly by 5% to reduce the low biases of those winds. Both QuikSCAT and ASCAT attenuate at high winds and care must be taken in weighting these observations in the variational analysis discussed in section 3. Throughout the remainder of this paper SCAT & ASCT will refer to scatterometry-based winds from QuikSCAT and ASCAT, respectively.

[1] QuikSCAT stopped transmitting data in November 2009

1.2. Satellite-based "flight-level" wind estimates

Cloud (CDFT) and water vapor (WV) feature track winds from geostationary satellites are also utilized at pressure levels below 600 hPa. These winds were provided by two agencies; NRL, Monterey which provides wind fields from international agencies (JMA, BOM, and EU METSAT), and NESDIS who creates winds in the Western/Eastern Pacific and Atlantic basin. These winds are treated as being at one uniform pressure level (i.e., flight-level) in the analysis. CDFT winds are primarily located in the region surrounding the tropical cyclone because high cloud cover often prevents tracking of low-level features closer to the TC center.
Flight-level winds associated with tropical cyclones are also created from the Advanced Microwave Sounding Unit (AMSU). Special processing methods have been developed for creating AMSU-based temperature profiles and height fields (Knaff et al. 2000, Demuth et al. 2004, 2006). These height fields at 700 hPa and 850 hPa are then used to create 2-d wind fields around tropical cyclones (Bessho et al. 2006). These winds are created when the center of the AMSU swath is within 700 km of the TC location. Currently, three satellites (NOAA 15, 16, 18) provide AMSU data for this algorithm. Temporally coverage is typically once to four times a day. An example of this type of wind field for the case of Tropical Cyclone Phet (IO032010) on 2 June 2010 at 0952 UTC and utilized for the 18UTC analysis is shown in Fig. 2.1.

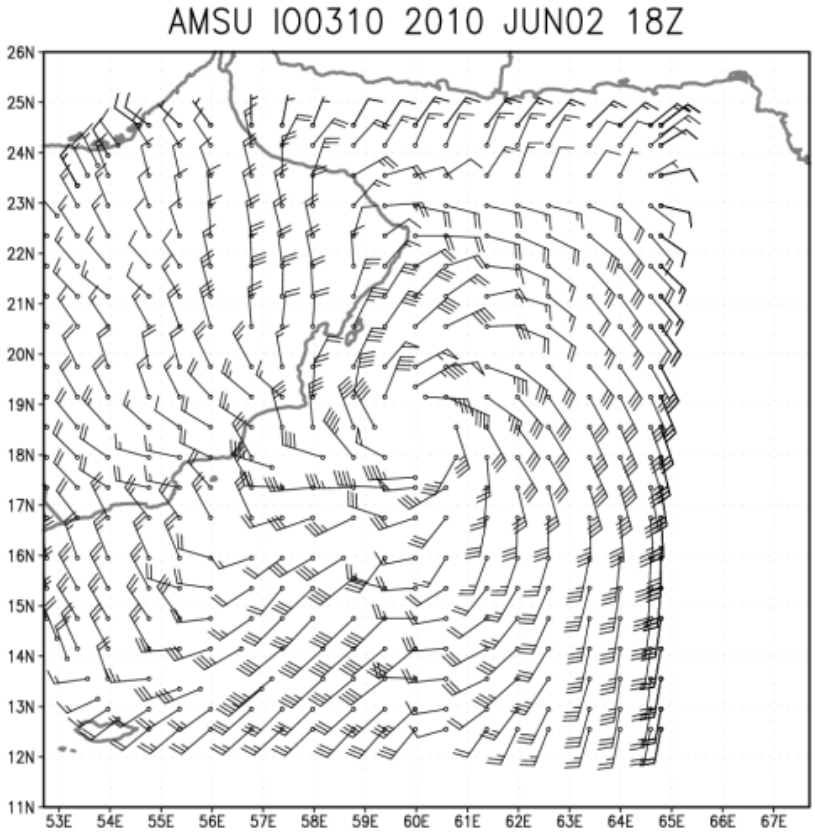

Figure 2.1. Example of AMSU 700 hPa winds from Tropical Cyclone Phet 2 June 2010 at 0952 UTC. The resolution is 0.2 degrees latitude/longitude and the winds have been thinned to show the wind barbs.

Notice in Fig. 2.1 that because of the AMSU instruments resolution (~50 km at Nadir), the winds within 100 km of the storm center are poorly estimated. As a result AMSU-based wind vectors are also weighted to minimize their errors on the final analysis. Despite the resolution-based shortcomings, these data are useful for determining the environment surrounding the storm and near storm asymmetries within the tropical cyclone vortex.

The winds in the inner region of the tropical cyclone are estimated using a method described in Mueller et al. (2006) that has been slightly modified for this application. The technique was developed on 10 years of coincident aircraft and infrared (IR) imagery. Aircraft data was binned in a storm relative manner over 12-hour periods and analyzed using a variation technique in a cylindrical framework. IR data came from a tropical cyclone satellite image archive maintained at the Cooperative Institute for Research in the Atmosphere (Kossin 2002). The method predicts the radius of maximum winds and wind speed at 182 km from the center given the storm intensity, location, and the IR imagery. From these parameters a modified Rankine vortex is fit. Asymmetries are added to this 1-d wind field using the storm motion. For this work the Mueller et al (2006) technique was modified 1) provide improved wind estimates in weak tropical cyclones and 2) to provide wind estimates out to 400 km radius. These winds henceforth will be referred to as IRWD. In real-time, storm intensity and location is estimated using information from the past operational estimates and forecasts. Extrapolation is used if no forecast exists. The estimate of maximum surface wind is a source of error, but is necessary to provide TC structure guidance prior to the creation of the operational analysis.

1.3. Data treatment

Both ASCT and SCAT wind estimates are surface observations (i.e., 10-m marine exposure, 1-minute average), but most of the other datasets used in this study are at flight level - in the lower atmosphere. For this reason SCAT data are adjusted to flight level (~ 700 hPa) by dividing by a flight-level-to-surface reduction factor that is a function of radius and then rotating the winds 20 degrees toward high pressure.

All of the datasets used are treated in a storm relative manner and are relocated using the storm motion vector to a common analysis time. All datasets are collected in this manner for a 12-h period prior to the analysis, except for the AMSU and scatterometer winds. AMSU 2-d winds and scatterometer winds are used for a 36-h period because they provide continuity on in the outer regions of the storm. However, all wind types receive less weighting (75% of the specified weighting) if they are older than 6 hours. More about the weighting of datasets is discussed below. To maintain a little continuity from one analysis to the next, the previous analysis is used as a first guess, if available. If used the first guess initial wind field has a small weighting relative to the input datasets. Finally, an analysis is attempted only if IRWD input data exist.

Algorithm

The multi-platform, storm-relative, flight-level dataset described in section 2 is used as input to an objective analysis system. The objective analysis is based upon the model-fitting approach with smoothness constraints described by Thacker (1988). In this approach, the difference between the data and the model counterpart of the data is minimized, where the model is simply the wind components on any evenly spaced grid. The model counterpart of the observations is a bilinear interpolation of the wind components to the location of the observation. The smoothness constraints help to fill in the data void areas of the analysis domain.

As an example, suppose there are K observations of a wind components u and v, denoted by u_k and v_k, and M observations of wind speed, denoted by s_m located at arbitrary locations with a domain $x \in [0,L_x]$, $y \in [0,L_y]$. For the objective analysis, the values of u, v and s on an evenly spaced x, y grid with grid spacing of Δx, Δy (denoted by U_{ij}) are determined by minimizing the cost function C defined by

$$
\begin{aligned}
C = & \frac{1}{2}\sum_{k=1}^{K} w_k \left[(u_k - U_k)^2 + (v_k - V_k)^2 \right] \\
& + \sum_{m=1}^{M} w_m (s_m - S_m)^2 \\
& + \sum_{i=1}^{I}\sum_{j=1}^{J} \left\{ \begin{array}{l} \alpha\left[(\delta_{xx} U_{ij})^2 + (\delta_{xx} V_{ij})^2\right] \\ + \beta\left[(\delta_{yy} U_{ij})^2 + (\delta_{yy} V_{ij})^2\right] \end{array} \right\}
\end{aligned}
\qquad (1)
$$

, where δ_{xx} and δ_{yy} are the discretized second derivative operators where

$$\delta_{xx} U_{ij} = (U_{i+1,j} + U_{i-1,j} - 2U_{ij})/\Delta x^2 \quad ,$$

and

$$\delta_{yy} V_{ij} = (V_{i+1,j} + V_{i-1,j} - 2V_{ij})/\Delta y^2$$

, respectively.

In (1) U_k and V_k are the component wind values bi-linearly interpolated from the analysis grid to the observation point k, w_k are data weights, α and β are smoothness parameters, and i and j are the number of analysis points in the x and y directions. Similarly, S_m are the wind speed values interpolated to the observation point m, w_m are the data weights for the wind speed. The first three terms on the right side of (1) measures the misfit between the analysis and the observations and the second term is a constraint that acts as a low-pass filter. As shown by DeMaria and Jones

(1994) for the one-dimensional case, the filter response function F (k) for the constraint term in (1) can be written as

$$F(k) = 1/\{1 + 8\alpha[1 - \cos(k\Delta x)]^2\} \quad , \quad (2)$$

where F(k) is the amplitude reduction factor of a pure cosine wave with wavenumber k. Because α is in the denominator in (3) it controls the amount of smoothing. For example, for the $2\Delta x$ wave on the analysis grid ($k=2\pi/2\Delta x$), the amplitude will be reduced by a factor of $(1+32\alpha)^{-1}$. Thus, α and β can be chosen to be consistent with the data coverage relative to the analysis grid spacing. In the analysis code, the fields U_{ij}, V_{ij} and S_{ij} that minimized C is found using a simple steepest descent algorithm, which requires the calculation of the gradient of C with respect to U_{ij} and V_{ij} . Given the simple form of (1), the gradient is calculated using an analytic formula.

The objective analysis is formulated in cylindrical coordinates with 200 radial points ($\Delta r=4.5$ km) from r=2 to 902 km and 36 azimuthal points ($\Delta\theta=10^o$), and the wind components are input as radial and tangential values. An advantage of the cylindrical system is that different smoothness constraints can be applied in the radial and tangential directions. In this formulation, α and β are the half-power filter wavelengths in the radial and tangential directions.

Different weights (i.e., w_k, w_m) are also applied to the datasets. Weighting of the individual data types is based on the average H*wind (Powell et al. 1998) errors. AMSU, WV and CDFT inputs have constant weights. IRWD and SCAT weights are functions of both radius (r) and maximum winds (vmax). To facilitate the estimation of weights we define,

$$vf = 1 + (v\max - 50)/65$$
$$wt_{ir} = 0.35 * vf,$$
$$wt_{scat} = 0.45 * vf,$$
$$dist_{scat} = 50 * vf,$$

where $dist_{scat}$ has units of km. The weights for AMSU and SSMI winds are set to the constants 0.13 and 0.5, respectively. The weights for the IRWD are defined by

$$W_{irwd} = wt_{ir} - 0.000125 * r * vf^2,$$

which decrease with increasing radius and have smaller values for storms with maximum intensities less than 50 kt. The weights for SCAT/ASCT winds are defined by

$$W_{scat} = MIN(0.60, wt_{scat} + vf(r - dist_{scat}) * 0.0004), r \geq dist_{scat} \quad .$$

For the SCAT/ASCT winds occurring within $dist_{scat}$ of the TC center the wind speed weights (i.e., w_m's in equation 1) are equal to the wt_{scat} and the weights to the wind speed components (i.e. w_k's in equation 1) are set to zero. Examples of the wind component weights and wind speed weights for each product is shown as a function of radius for three different intensities in Figure 2.2.

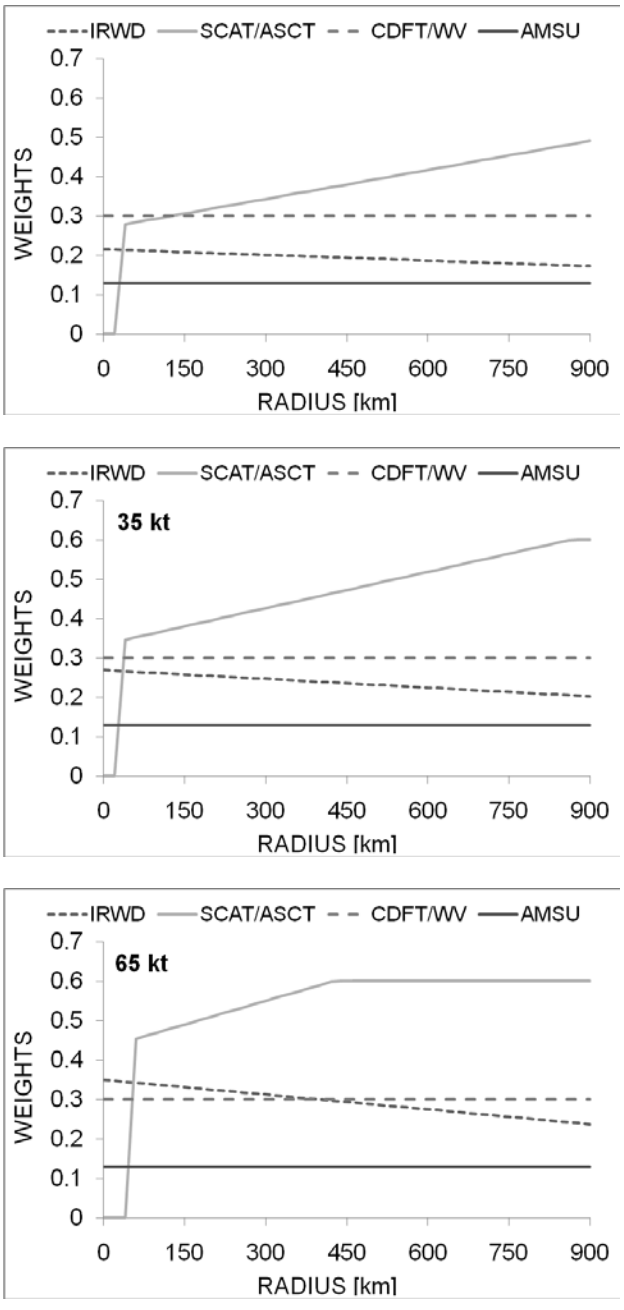

Figure 2.2. The panels show examples of data weights as a function of data type, radius and intensity. Note that all weights for storms with intensities greater than 65kt have the same weights as the lower panel.

Notice that satterometry-based winds are generally weighted most in the analysis and increase as a function of radius. IR winds have the second largest weighting in the analysis and decrease as a function of radius. SCAT /ASCT and IRWD weights also decrease and increase, respectively near the storm center and with higher intensities. CDFT/WV inputs are weighted fairly heavily, but are often unavailable near the TC center. The AMSU-based winds are weighted in a moderate manner, but are almost always available for the entire domain. The favoring of the SCAT/ASCT wind vectors is somewhat noteworthy given the findings in Hennon et al. (2006) and may suggest that the their findings were based on a sample of stronger tropical cyclones.

The variational analysis is actually run three times, which allows for some additional quality control. The first analysis uses fixed α and β. Using this first smooth analysis a gross quality control is applied to remove obviously errant data from subsequent analyses. For the two remaining analyses, α and β were chose so that the half power wavelengths of the filter were 22.5 km in radius and 100^o in azimuth within 300 km of the center, becoming equally weighted (~350 km) when 500 km or greater from the center. Again a gross quality control is applied between the second and final analysis. For each quality control step the threshold for the quality control is a function of the maximum observed wind speed as shown in Table 2.2. If the threshold is exceeded the data weights are simply set to zero.

Table 2.2: Gross quality control applied between the second and final analyses.

Gross Quality Control Pass	Function [kt]
First – prior to the second analysis	MAX(7.0,0.20*Vmax)
Second –prior to the final analysis	MAX(3.5,0.10*Vmax)

Once the various satellite wind data are analyzed to a common level (at ~700 hPa), a marine exposure surface wind reduction is applied (i.e., to estimate the 10-m, 1-minute wind vectors). The reduction factor is assumed to be 0.9 within 100 km of the TC center. From that radius, the reduction factor decrease linearly to a value of 0.75 at 700 km. Beyond 700 km from the TC center the reduction factor remains at 0.75. These reductions are consistent with the findings of Franklin et al. (2003) – it is assumed that the inner 100km is convectively active. The resulting winds are also turned toward low pressure by 20^o. A land mask is then used to determine if the observation is over land. If the wind observation is over land, an additional 80% reduction is applied and the winds are turned an additional 20^o following Boose, et al. (2001) for a total turning of 40^o. The flight-level to surface reductions for location over over-water and over-land are shown in Fig. 2.3 as a function of radius.

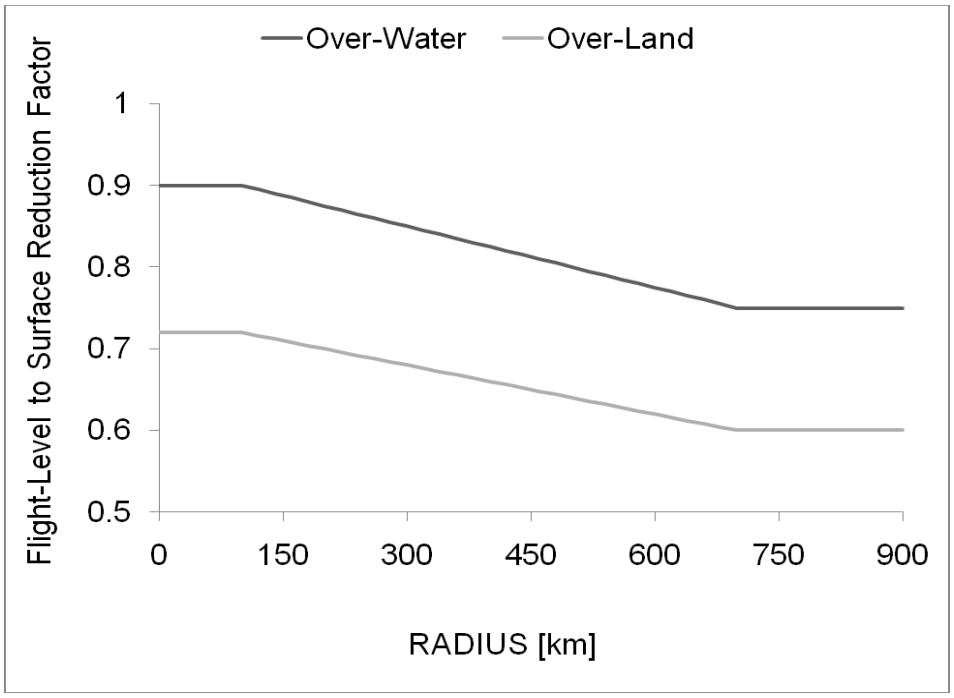

Figure 2.3. The flight-level to surface reduction factors used in MTCSWA for over-water and over-land conditions.

Finally MSLP estimates are created by integrating the resulting azimuthally averaged wind at flight-level (considered gradient level) from 600 km inward. Estimates of the SLP at 600 km come from the NCEP AMSU anlyses (GFS based).

2. Product Description

The MTCSWA product is disseminated through the product website (http://www.ssd.noaa.gov/PS/TROP/mtcswa.html). The products range from graphical information to text data and include all of the information needed to reprocess the input data.

2.1. Graphical Products

There are nine graphical products. These include eight products displayed on the web page, namely the surface wind analysis (storm scale), the surface wind analysis (inner core scale), AMSU data used in the analysis, CDFT/WV data used in the analysis, IRWD data used in the analysis, SCAT/ASCT data used in the analysis, a time series of maximum winds and MSLP and an infrared image of the TC at analysis time. The final graphical product provides the Kinetic Energy within 200km of the cyclone center at flight-level, plotted against the intensity. The scale for KE is provided in Maclay et al. (2008) and has been related to damage potential. Examples of the graphical products for Hurricane Celia (EP0410) on 21 June 2010 at 00UTC are shown in Figure 3.1.

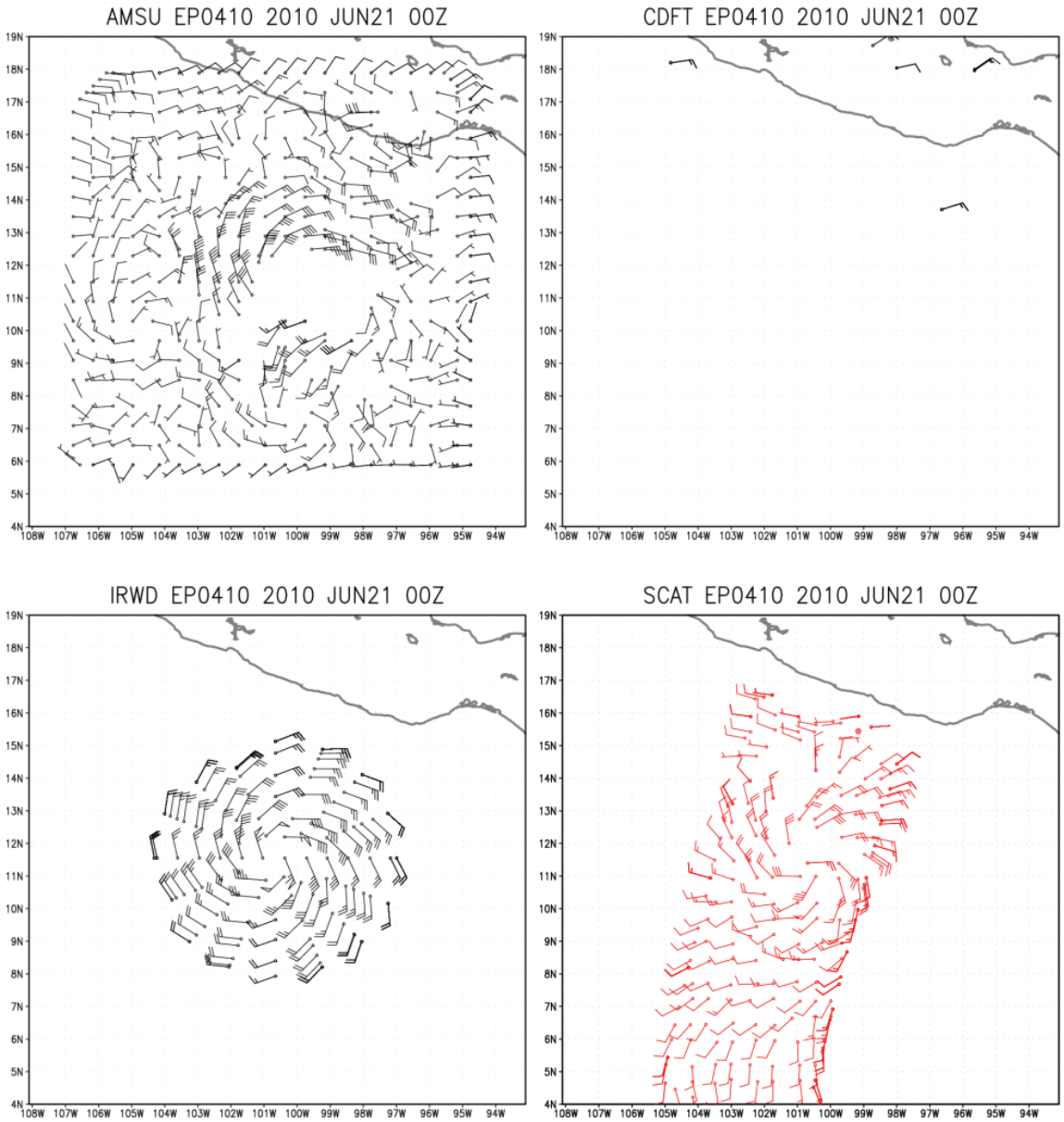

Figure 3.1. Examples of graphical products generated for Hurricane Celia (EP0410) . Shown are the basic input datasets, namely AMSU, CDFT, IRWD, and ASCT.

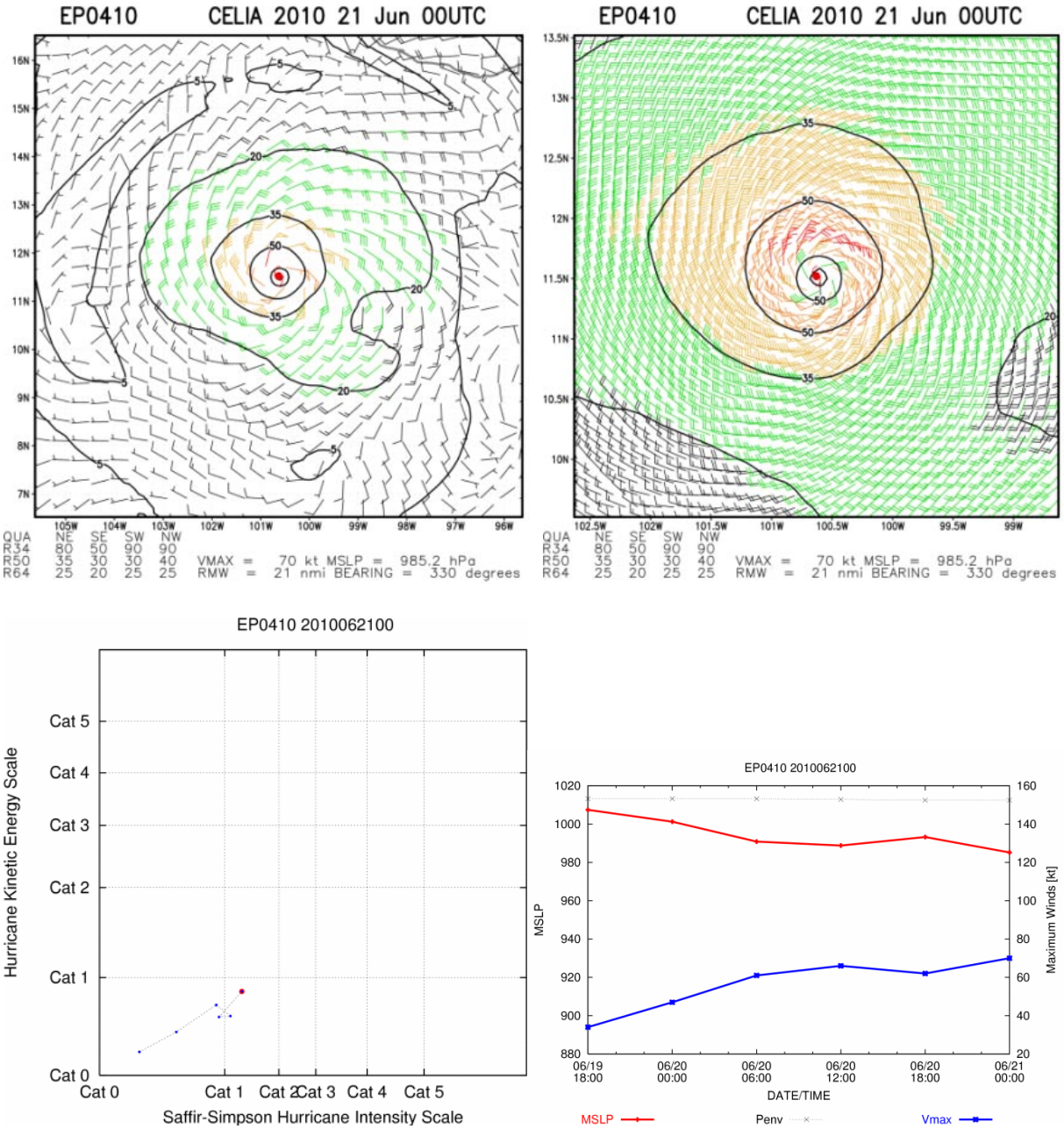

Figure 3.1 (cont). The wind analysis is created at two different scales as shown in the top two panels. The bottom panels show the time series of the integrated kinetic energy (0-200km) vs. current intensity, and the time series of the analyzed maximum wind speed and estimated minimum sea level pressure (MSLP).

2.2. Text Products

A number of ancillary data files are also generated that contain input, output and diagnostic information. These are available from the archive ftp site

(ftp://satepsanone.nesdis.noaa.gov/MTCSWA). A complete list of files included in the archive is listed in Table 3.1. All files use the following naming convention,

Year Product Type Time Period
yyyyBBNN_MTCSWA_YYYYmmddHH.prd
where,
yyyy is the storm year
BB is the storm basin (AL,EP,CP,WP,IO,SH)
NN is the storm number
MTCSWA is the product name
YYYY is the year of the analysis
mm is the month of the analysis
dd is the day of the analysis
HH is the hour of the analysis.
prd is the product naming convention

which is also utilized in Table 3.

Table 3.1. A comprehensive list of text/binary files produced by the MTCSWA product is provided. These will also be archived at NCDC.

Naming Convention	File Type	Contents
yyyyBBNN_MTCSWA_YYYYmmddHH.AAV	Output (ASCII)	azimuthally averaged surface and gradient level winds. ASCII file with header
yyyyBBNN_MTCSWA_YYYYmmddHH.DIA	Diagnostic (ASCII)	wind/MSLP diagnostics used for storm surge modeling
yyyyBBNN_MTCSWA_YYYYmmddHH.FIX	Output (ASCII)	ATCF-formatted fix that is supplied to NHC/JTWC
yyyyBBNN_MTCSWA_YYYYmmddHH.KE	Output (ASCII)	estimates the 0-200km Kinetic Energy at flight-level, the radius of maximum winds and the surface maximum wind in the analysis
yyyyBBNN_MTCSWA_YYYYmmddHH.LOG	Output (ASCII)	the status and latency of the various input datasets
yyyyBBNN_MTCSWA_YYYYmmddHH.MSL	Output (ASCII)	the environmental sea-level pressure used and the estimated Minimum Sea-level Pressure
yyyyBBNN_MTCSWA_YYYYmmddHH.PEN	Output (ASCII)	Contains an estimate of environmental pressure at r=600 km (Usually from GFS)

yyyyBBNN_MTCSWA_YYYYmmddHH.SFC	Output (ASCII)	the surface wind analysis. This ASCII file contains date/time, lat, lon, u, v in kts on the cylindrical analysis grid
yyyyBBNN_MTCSWA_YYYYmmddHH.STATUS	Diagnostic (ASCII)	information about when the analysis ran and how successful it was
yyyyBBNN_MTCSWA_YYYYmmddHH.WIN	Output (ASCII)	the flight-level wind analysis on an azimuthal grid defined in the file
yyyyBBNN_MTCSWA_YYYYmmddHH.bin	Output (binary, big endian)	GrADS binary file that contain gridded surface and flight-level winds
yyyyBBNN_MTCSWA_YYYYmmddHH.ctl	Output (ASCII)	Grads control file
yyyyBBNN_MTCSWA_YYYYmmddHH.inp	Input (ASCII)	contains the storm input estimates at the time of the analysis, which come from the ATCF and are generated prior to the start of the analysis
yyyyBBNN_MTCSWA_YYYYmmddHH.obs	Input (ASCII)	containing the winds used in the analysis. These come from IR-based flight-level proxy winds, AMSU non-linear balance winds, Geostationary based cloud and feature track winds, and scatterometry (ASCT and SCAT)

One file created, the ATCF (Sampson and Schrader 2000) formatted fix, is of particular interest to operational users. This file appears in the archive, but is also mirrored for a short duration at ftp://satepsanone.nesdis.noaa.gov/MTCSWA/ATCF_FIX/. Operational centers can grab it and ingest this file in real-time.

3. Product Verification

Since tropical cyclone surface wind field estimates are considered most accurate when aircraft reconnaissance is available, the MTCSWA Product is verified using two different datasets. The first dataset is to use the H*Wind analyses (Powell et al. 1998) obtained from the Hurricane Research Division (HRD). The H*wind analyses of the 2-d wind field makes use of surface winds from buoys, station observations, ships, satellite-cloud drift winds in addition to aircraft

reconnaissance data at flight-level and at the surface via stepped frequency microwave radiometer. The second verification dataset is the significant wind radii and minimum sea level pressure (MSLP) from the best track analyses from NHC and from wind radii and MSLP from climatology. The wind radii climatology comes from Knaff et al. (2007) and the MSLP climatology is based on a fit to the Dvorak (1975) Atlantic wind-pressure relations using a quadric function of the maximum wind speed provide by Knaff and Zehr (2007). The comparison of wind radii and MSLP will be done when aircraft reconnaissance is within ± 2 hours of the surface wind estimate. Both verifications were conducted during the years 2008-2009 when the MTCSWA algorithm was fixed and SFMR surface wind estimates were operational.

3.1. H*Wind Comparisons

Comparisons between MTCSWA and H*Wind analyses were conducted in a storm relative coordinate system. The closest H*wind analysis with respect to time was used for the comparisons. The cylindrical grid of the MTCSWA were compared with H*Wind analyses that were interpolated to the same cylindrical coordinate system. The two analyses were centered at the same location. Spatial mean absolute errors (MAEs) and biases were then calculated. In the 2008-2009 period there were 250 coincident H*wind and MTCSWA analyses, which not only allowed for a large representative sample of cases for our analysis, but allowed further stratification by intensity.

Figure 4.1 show the MAEs and biases associated with the analysis of all 250 coincident cases. The MAEs are the largest within 50 km the center of the cyclone where errors exceeded 5 ms^{-1}. Elsewhere MAEs are smaller than 5 ms^{-1} and appear roughly symmetric about the storm center. The biases show a tendency to slightly overestimate in the northwest quadrant of the storm within 100 km and to slightly underestimate the winds on the southeast quadrant between approximately 120 and 250 km from the storm.

We next examine the MAEs and biases as a function of TC intensity. Figure 4.2 shows MAEs and biases stratified by tropical depressions and tropical storms, and Fig. 4.3 shows the same analyses for minor hurricanes (64-95 kt), and major hurricanes (>95 kt). In the case of tropical depressions where there are 16 cases, the MAEs seem to be related to biases in the wind field. Specifically it appears that the MTCSWA maximum winds are too widely spread and symmetric. This should be somewhat expected given the IRWD input, which is heavily weighted near the storm center, and is composed of a symmetric wind model. The MAEs associated with tropical storms are generally much lower than for tropical depressions, with most of the analysis domain having MAEs less than 5 ms^{-1}. The biases for the tropical storm cases are beginning to show the wavenumber one pattern shown for the all cases sample. There is also some indication that most of the errors are related to positioning of the radius of maximum winds, with negative biases nearest the center surrounded by a ring of positive biases.

The MAEs and biases associated with hurricanes with intensities less than 95 kt are shown in Fig. 4.3. In these cases the MAEs are largest around the region where the radius of maximum winds is typically located. However there is a region to the west of the storm where errors

exceed 5 ms^{-1} that are associated with the larger negative biases in those regions. The major hurricane cases, also shown in Fig. 7 show again that the positioning of the radius of maximum with is the primary source of errors. High biases are located within about 100km of the center. It is thought that this is due to the inability of the Rankine vortex used in the IRWD to represent the often very steep increase of the winds as one moves inward toward the radius of maximum winds. It appears however that beyond 100 km the other datasets helps to reduce this bias. The consistent wave number one patterns in the biases suggest that one of the input data sets is the likely cause. After examination, the AMSU winds are the likely culprit. This negative bias southeast of the TC center is thought to result of 1) global model (GFS) boundary conditions and 2) the Beta-plane assumption made when calculating the non-linear balance approximation winds.

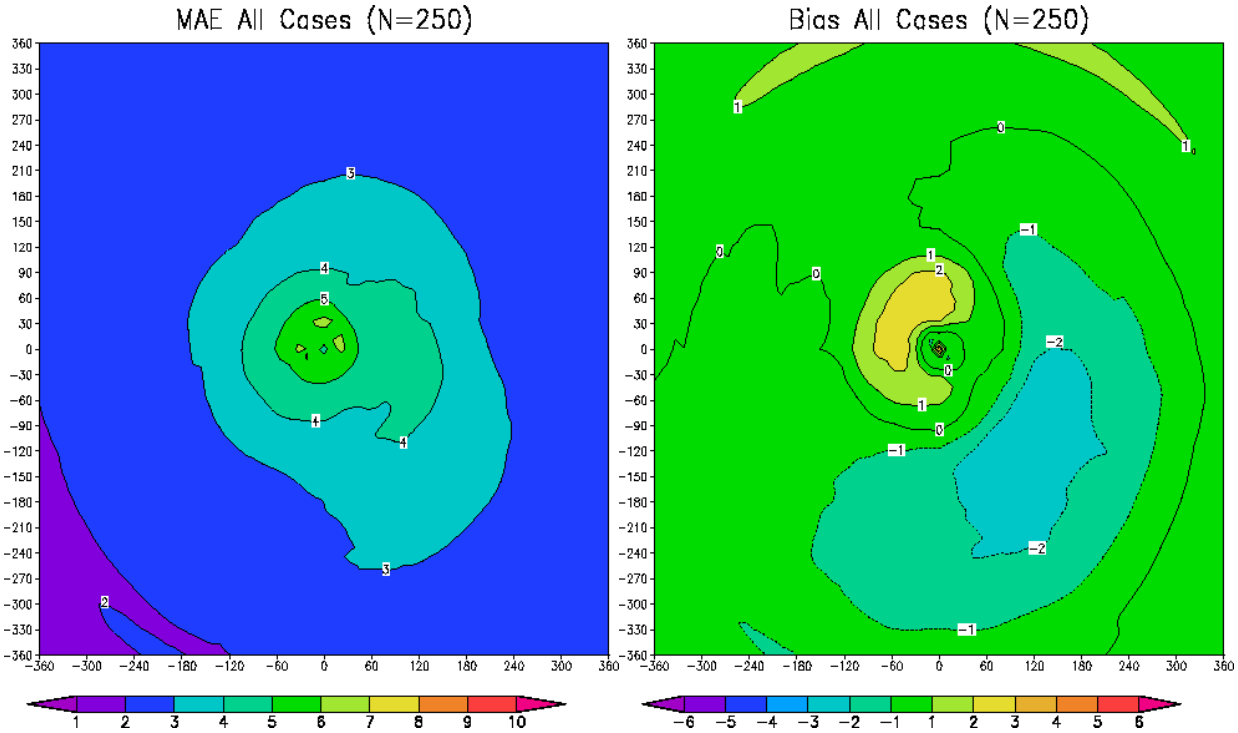

Figure 4.1. The MAEs and biases associated with the MTCSWA for all cases with coincident (±3 hours) H*wind analyses. H*Wind is assumed ground truth, and centers of the two analyses are collocated. Units are ms^{-1}.

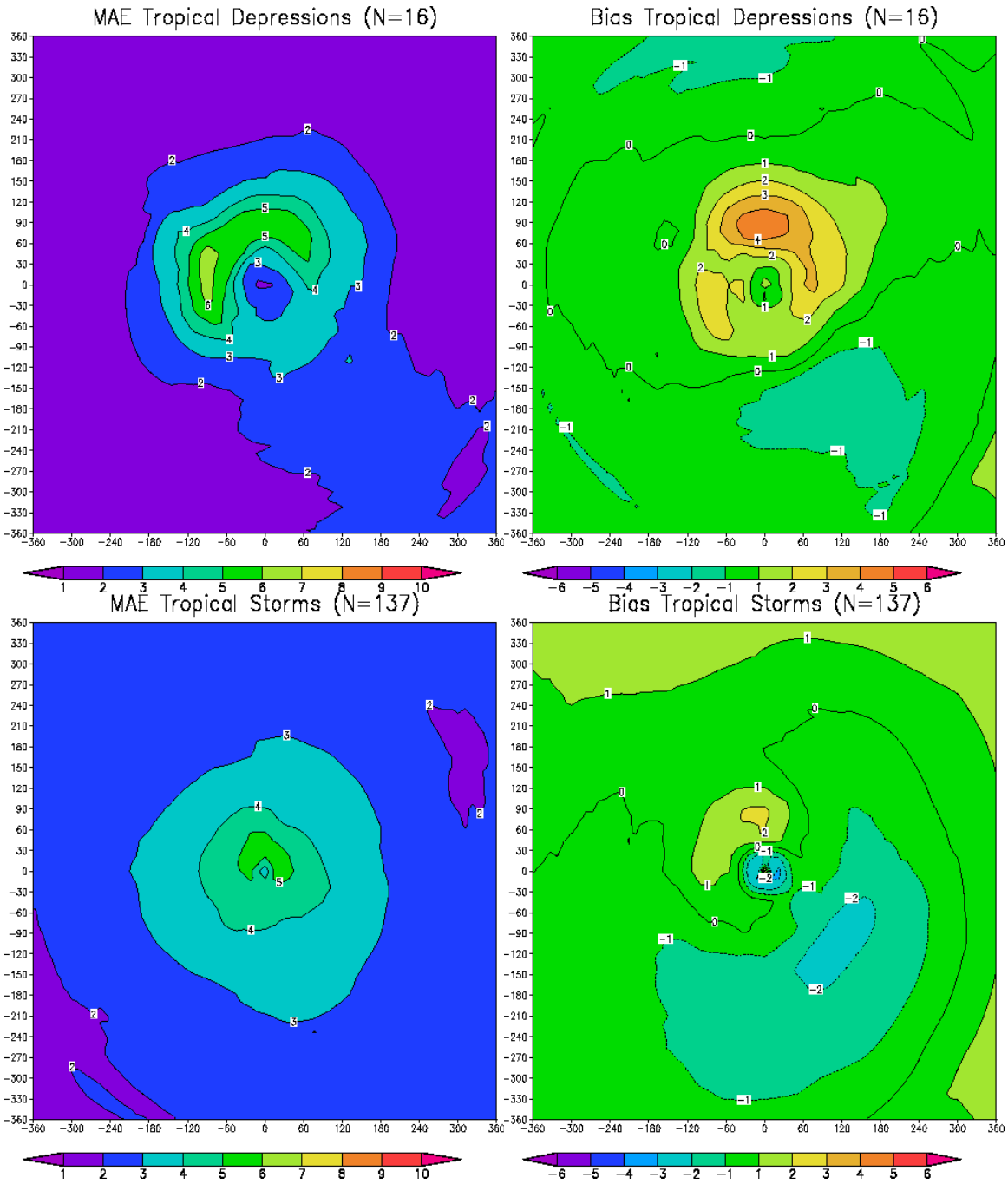

Figure 4.2. Same as Fig.4.1, except for tropical depressions cases (top) and tropical storm cases (bottom).

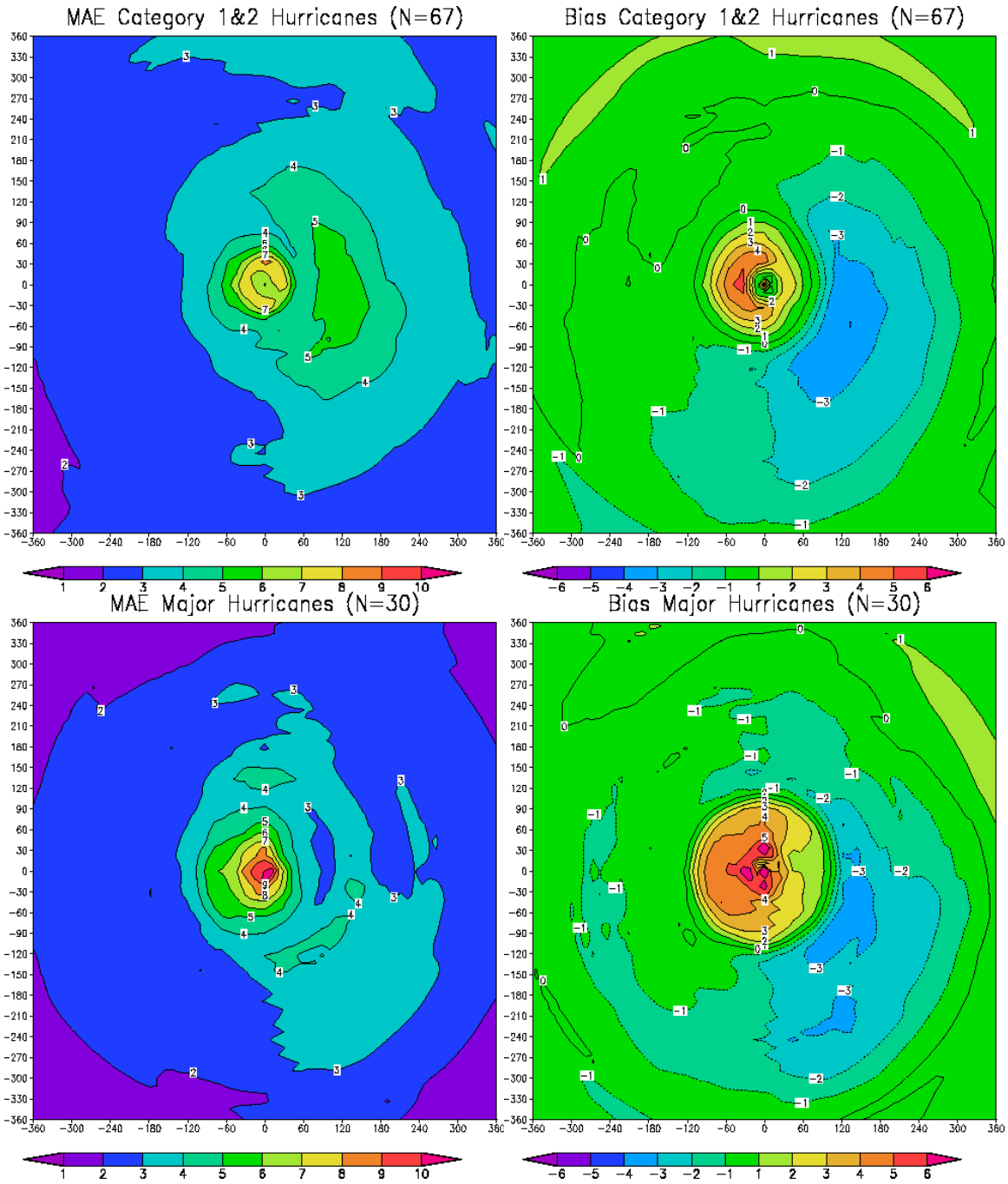

Figure 4.3. Same as Fig.4.1, except for hurricanes (i.e., < 95 kt) cases (top) and major hurricane cases (bottom).

To complete this analysis it is informative to compare the above results to the MAEs associated with the raw input data used in the MTCSWA. Figure 4.4 shows the azimuthal mean MAE's associated with the five of the inputs (IRWD, AMSU, ASCT, QSCT, CDFT) for all hurricane cases (top) and non-hurricane cases (bottom). Note that errors are calculated on a cylindrical grid and that MAE values are not shown in Fig. 4.4 if the number of points is less than 30. This comparison, which uses the same cases used in Figures 4.1-4.3, clearly shows that the MTCSWA

product produces MAEs smaller than any of the individual inputs and thus not only combines the input data information, but adds value by decreasing the potential analysis errors.

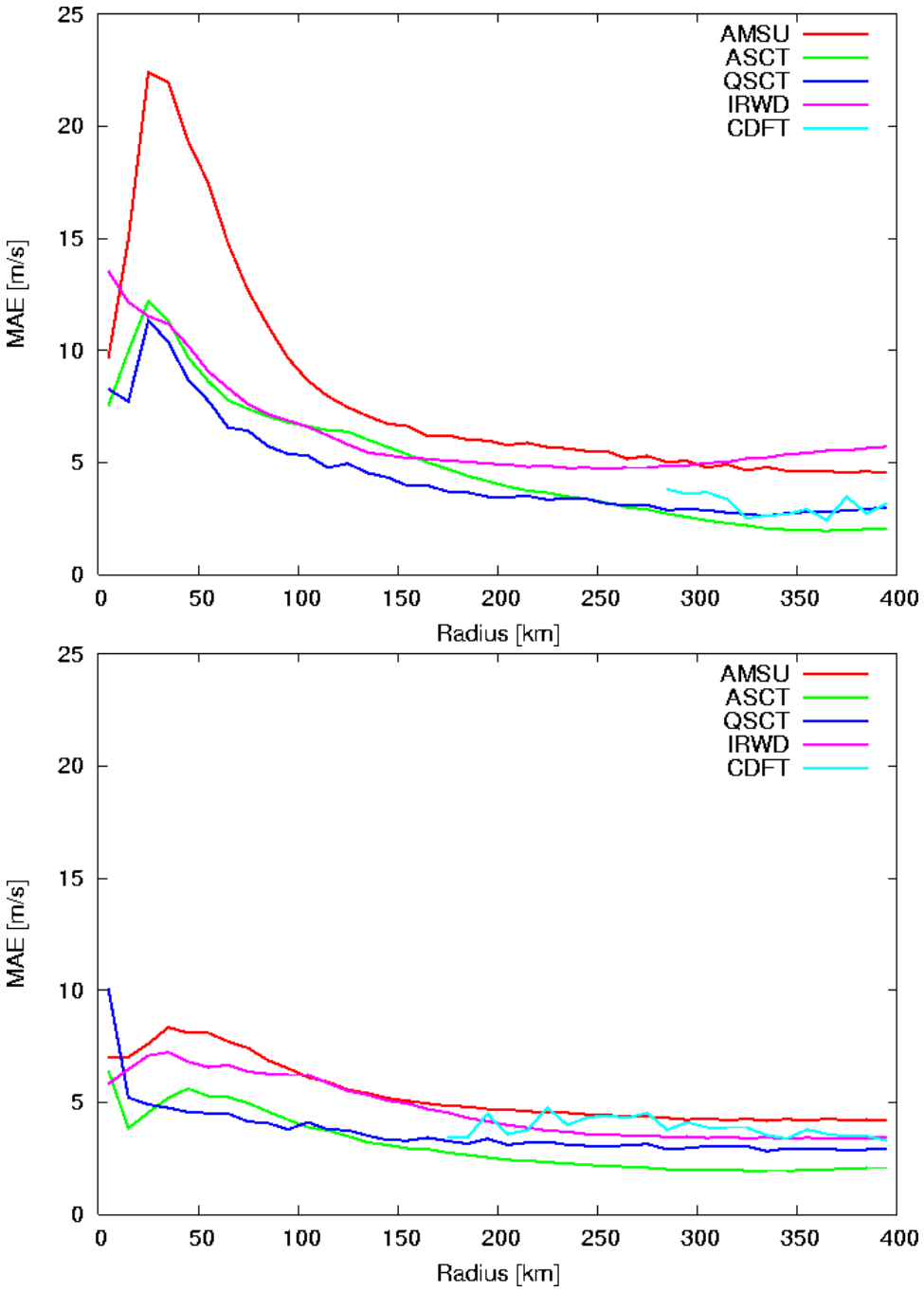

Figure 4.4. Azimuthal mean MAE associated with the input datasets used in the MTCSWA product. All hurricane cases (≥64 kt) are shown on the top and All non-hurricane (<64 kt) are shown at the bottom. H*wind cases are used as ground truth and the same 2008-2009 sample is used.

3.2. Wind radii and MSLP comparisons

Using the same 2008-2009 sample we compare the MTCSWA-based wind radii and MSLP estimates to the estimates in the best track files and those estimated by climatology. The best

track files contain the best estimates of intensity, MSLP, and wind radii associated with a given tropical cyclone at roughly a 6 hourly frequency. Best tracks are finalized post season and are reanalyzed using all available information. Because there are relatively few tools to estimate wind radii, errors associated with the best track estimates may be as high as 30% (James Franklin, personal communication). These comparisons were nonetheless calculated for all Atlantic cases within ± 2 hours of aircraft observed/estimated MSLP as well as all periods during 2008 and 2009. The verification considers wind radii in the northeast, southeast, southwest and northwest quadrants as well as in all quadrants. Because of the stepped quantification of wind radii, the all quadrants wind radii compares the average of the non-zero wind radii and thus is a general measure of TC size. Many statistics were calculated [MAE, bias, RMSE, R^2, false alarm rate (FAR), and probability of detection (POD)], but this discussion will concentrate on the aircraft-only MAE, bias, and R^2 statistics to emphasis MTCSWA performance vs. climatological estimates of both wind radii and MSLP (as a function of intensity). Note that MAE verification results to include wind radii estimates of zero (i.e., no wind radii in the quadrant).

Figure 4.5 show the MAE and biases associated with the radii of 34-, 50- and 64-knot (kt) wind radii based on aircraft influenced cases. The units, nautical miles (n mi, where 1n mi = 1.85 km), match those used in operations. The MTCSWA wind radii estimates perform well against climatology. In most cases the MAEs are smaller for the MTCSWA estimates, and those estimates seem to perform better than climatology for the more important hurricane (64-kt) and 50-kt wind radii. Biases indicate that the negative biases in the east quadrants shown in the H*wind comparisons carry over to the wind radii in the NE and SE quadrants that underestimated, though it is interesting to note that climatology also has similar biases. This result highlights the sensitivity of wind radii estimates to the analyzed wind speeds in that small radial changes in wind speed can result in quite large differences in wind radii estimates. The hurricane force wind radii also show a tendency to have a slight high bias as would be expected due to errors associated with the radius of maximum wind shown in the previous section and the known limitations of the IRWD input data, but its biases are a large improvement over climatology.

The MTCSWA-based wind radii generally explained larger amounts of variance than their climatological corresponding climatological estimates, shown in Fig. 4.6. This result is even holds true for the hurricane strength wind radii. This result indicates that the MTCSWA-based wind radii provide, not only have smaller MAE, but also capture important aspects about the asymmetries of the wind fields around tropical cyclones. The larger variance explained by the non-zero averaged wind radii (i.e., ALL in the plots) also indicates that MTCSWA captures more of the general vortex size variations. The FAR and POD statistics between the MTCSWA and climatological estimates of wind radii were found to be statistically similar, not shown.

The final parameter examined in this analysis was the MSLP. To do this we used the Dvorak (1975) wind-pressure relationship as climatology, which is the accepted climatological relationship for the Atlantic Basin. We then compared those values to estimates made by integrating the azimuthal mean wind field produced by the MTCSWA Product. Those results of the analysis are shown in Table 4.1. The results show that the MTCSWA provides slightly improved estimates of MSLP. Furthermore, since the MSLP is an integrated measure of the wind, this shows that the MTCSWA is producing a dynamically consistent wind field.

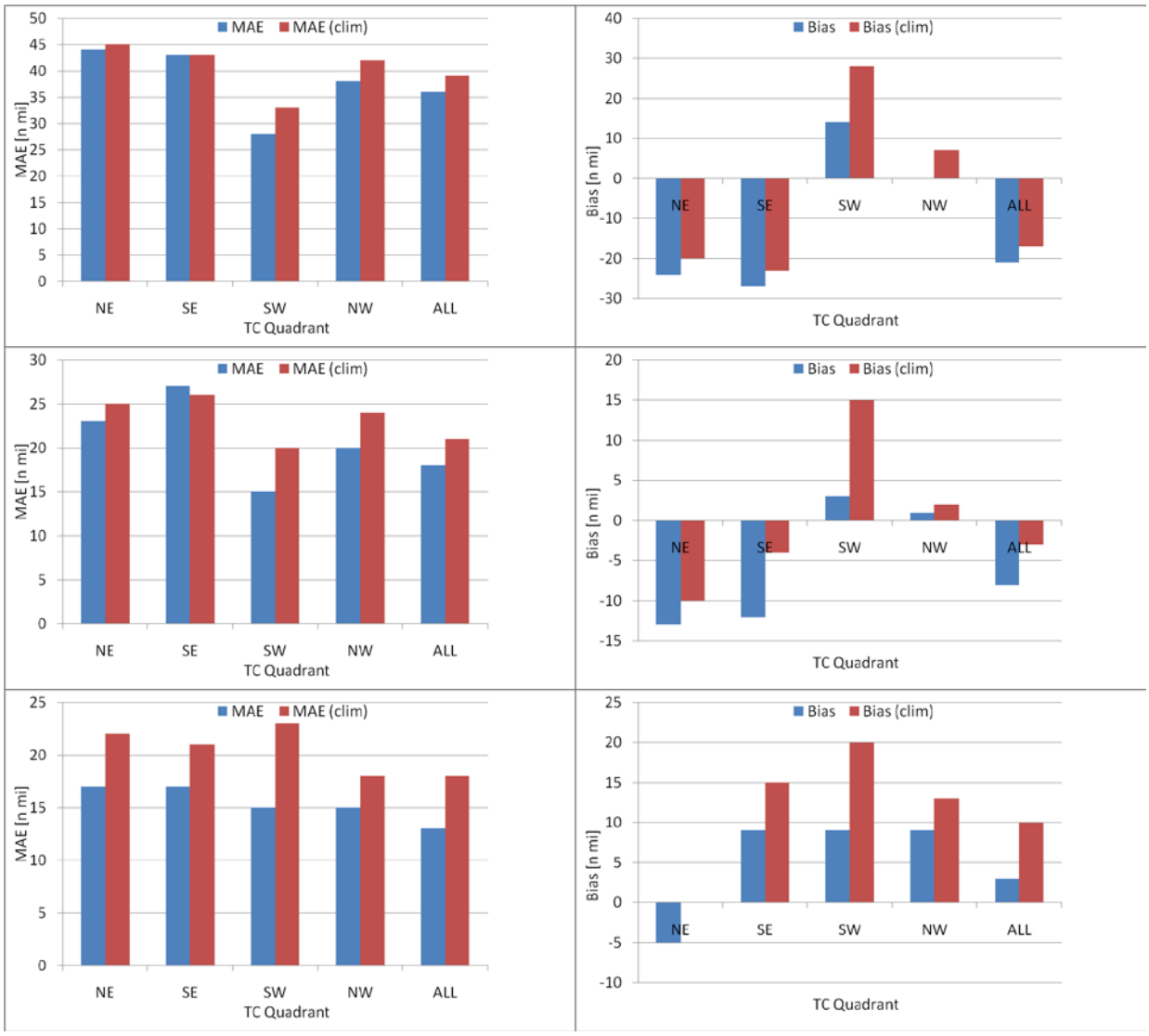

Figure 4.5. MAE and bias associated with the wind radii estimates of the MTCSWA product and that of climatology. MAEs are given in the left panels and bias in the right panels. Results for the gale force wind radii are provided at the top, 50-kt wind radii in the middle and hurricane force wind on the bottom rows and the number of cases analyzed is 129, 79 and 59 respectively.

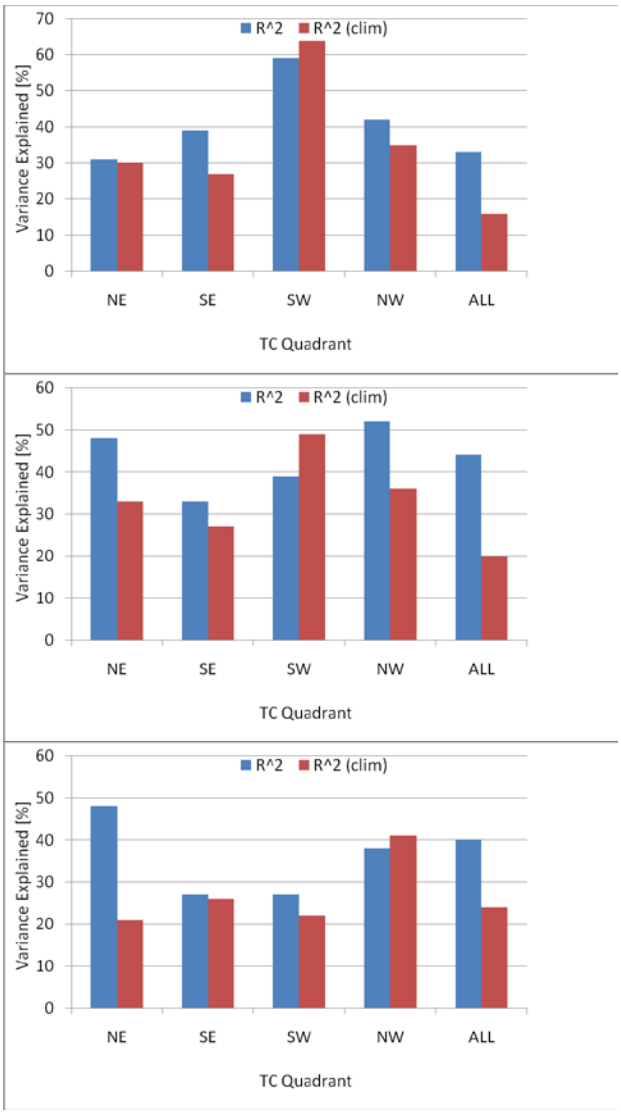

Figure 4.6. Percent variance explained by wind radii estimates from the MTCSWA Product and from Climatology (Knaff et al. 2007). Results are shown for gale force (34-kt, top left), 50-kt (top right) and hurricane force (64-kt, bottom left) wind radii.

Table 4.1. The verification statistics comparing the MSLP estimated by the MTCSWA Product with those estimate from the Dvorak (1975) climatology. Units are hPa.

	MTCSWA	**Climatology (Dvorak 1975)**
Bias	0.5	2.4
MAE	6.8	7.0
RMSE	9.5	9.2
R^2 [%]	84	82

References

Bentamy, A. (2008). Characterization of ASCAT measurements based on buoy and QuikSCAT wind vector observations. *Ocean Sci. Discuss.*, **5**, 77–101.

Bessho, K., M. DeMaria, J.A. Knaff, 2006: Tropical Cyclone Wind Retrievals from the Advanced Microwave Sounder Unit (AMSU): Application to Surface Wind Analysis. *J. Climate Appl. Meteor.,* **45**, 399 - 415.

Boose, E. R., K. E. Chamberland, D. R. Foster, 2001: Landscape and regional impacts of hurricanes in New England. *Ecological Monographs*, **71**, 27-48.

Cobb, H. D., III, R. Knabb, P. S. Chang, and Z. Jelenak, 2008: Preliminary assessment of the utility of ASCAT ocean surface vector wind (OSVW) retrievals at the Tropical Prediction Center/National Hurricane Center. Preprints, *28th Conf. on Hurricanes and Tropical Meteorology, Orlando, FL, Amer.* Meteor.Soc., 15B.4. [Available online at http://ams.confex.com/ams/pdfpapers/137882.pdf.]

DeMuth, J.L., M. DeMaria, J.A. Knaff, and T.H. Vonder Haar, 2004: Evaluation of advanced microwave sounder unit (AMSU) tropical cyclone intensity and size estimation algorithm, *J. App. Met.*, **43**, 282-296.

Demuth, J., M. DeMaria, and J.A. Knaff, 2006: Improvement of Advanced Microwave Sounding Unit Tropical Cyclone Intensity and Size Estimation Algorithms, *J. Climate Appl. Meteor.*, **45**, 1573–1581.

DeMaria, M., and R.W. Jones, 1993: Optimization of a hurricane track forecast model with the adjoint model equations. *Mon. Wea. Rev.*, **121**, 1730-1745.

____, M. DeMaria, J. A. Knaff, and T. H. Vonder Haar, 2004: Validation of an advanced microwave sounder unit (AMSU) tropical cyclone intensity and size estimation algorithm, J. App. Met., **43**, 282-296.

Dvorak, V. F., 1975: Tropical cyclone intensity analysis and forecasting from satellite imagery. *Mon. Wea. Rev.,* **103,** 420–430.

EUMETSAT, cited 2010, ASCAT Wind Product User Manual. [Available online at http://www.knmi.nl/publications/fulltexts/ss3_pm_ascat_1.3.pdf]

Franklin, J. L. , M.L. Black, and K. Valde, 2003: GPS dropwindsonde wind profiles in hurricanes and their operational implications. *Wea. Forecasting*, **18**, 32-44.

Gaiser, P. W., 2004: The WindSat space borne polarimetric microwave radiometer: sensor description and early orbit performance. *IEEE Trans. Geosci. Remote Sens.*, **42**, 2347-2361.

Gelsthorpe, R. V., E. Schied, and J.J.W. Wilson, 2000: ASCAT- Metop's Advanced Scatterometer. ESA Bull., **102**, 19-27.

Graf, J.E.; Wu-yang Tsi; Jones, L., 1998: Overview of QuikSCAT mission-a quick deployment of a high resolution, wide swath scanning scatterometer for ocean wind measurement. Proceedings. IEEE Southeastcon '98. `Engineering for a New Era' (Cat. No.98CH36170), p. xiv+416, 314-317. [Available online http://ieeexplore.ieee.org/Xplore/dynhome.jsp]

Hennon, C.C., D. Long, and F. Wentz, 2006: Validation of QuikSCAT wind retrievals in tropical cyclone environments. *14th Conf. on Satellite Meteorology and Oceanography,* American Meteorological Society, Boston, MA. [Available online at http://ams.confex.com/ams/pdfpapers/99478.pdf]

Knaff, J.A., and R.M. Zehr, 2007: Reexamination of Tropical Cyclone Wind-Pressure Relationships. *Wea Forecasting*, **22**:1, 71–88.

Knaff, J.A., R.M. Zehr**,** M.D. Goldberg, and S.Q. Kidder, 2000: An example of temperature structure differences in two cyclone systems derived from the Advance Microwave Sounder Unit. *Wea. Forecasting,* **15**, 476-483.

Knaff, J.A., C. R. Sampson, M. DeMaria, T. P. Marchok, J. M. Gross, and C. J. McAdie, 2007: Statistical Tropical Cyclone Wind Radii Prediction Using Climatology and Persistence, *Wea. Forecasting*, **22**:4, 781–791.

Kossin, J.P., 2002: Daily hurricane variability inferred from GOES infrared imagery. *Mon. Wea. Rev*., **130**, 2260–2270.

Maclay, K.S., M. DeMaria and T.H. Vonder Haar, 2008: Tropical cyclone inner core kinetic energy evolution. *Mon. Wea. Rev*., **136**, 4882-4898.

Mueller, K. J., M. DeMaria, J. A. Knaff, J. P. Kossin, and T. H. Vonder Haar, 2006: Objective Estimation of tropical cyclone wind structure from infrared satellite data. *Wea. Forecasting*, **21**, 990–1005.

Powell, M.D. S. H. Houston, L. R. Amat, and N Morisseau-Leroy, 1998: The HRD real-time hurricane wind analysis system. *J. Wind Engineer. and Indust. Aerodyn.* **77&78**, 53-64.

Thacker, W. C., 1988: Fitting models to inadequate data by enforcing spatial and temporal smoothing. *J. Geophys. Res.*, **93**, 10655–10665.